Transaction A: Civil Engineering
Vol. 17, No. 3, pp. 169–183

SCIENTIA
IRANICA

Large-Scale Triaxial Testing and Numerical Modeling of Rounded and Angular Rockfill Materials

A. Aghaei Araei[1], **A. Soroush**[2,*] **and M. Rayhani**[3]

Abstract. *This paper studies the behavior of a number of blasting (angular) and alluvium (rounded) modeled rockfill materials by conducting large-scale triaxial testing, as well as numerical modeling. The numerical modeling is based on an elasto-plastic theory and enables one to predict the stress-strain-volumetric behavior of materials during shearing. The material parameters were determined from the experimental and numerical modeling. Variations of the material parameters, with respect to the confining pressure, Los Angeles abrasion, Point Load index, and particle breakage were investigated. Also, for design applications, curves fitted to the data are presented.*

Keywords: *Rockfill materials; Triaxial testing; Numerical modeling; Particle breakage.*

INTRODUCTION

Rockfill dams are increasingly used because of their inherent flexibility, capacity to absorb large seismic energy, and their adaptability to various foundation conditions. The use of modern earth and rockfill moving equipment and locally available materials make such dams economical as well. Rockfill materials consist primarily of angular to sub-angular blocks and particles obtained by blasting rocks or rounded to sub-rounded particles extracted from river beds.

The behavior of rockfill materials is affected by such factors as mineralogical composition, particle grading, fragmentation of particles, size and shape of particles, and stress conditions. Testing rockfill materials and modeling their behavior are essential prerequisites to realistic analyses and economic design of rockfill dams.

Rockfill materials contain particles of large sizes and their testing requires equipment of formidable dimensions. Therefore, the sizes of particles for testing are reduced, usually using modeling techniques. Four modeling techniques are available: the scaling technique [1], the parallel gradation technique [2], the generation of quadratic grain-curve technique [3] and the replacement technique [4]. Among them, the parallel gradation technique has been considered most appropriate by Ramamurthy and Gupta [5].

In high rockfill dams, particles of an underlying layer may be broken due to high stresses induced by the upper layers. Particle breakage and crushing of large particles to smaller ones result in lower strength and higher deformability. In earthquake prone regions, the latter is favored, as far as the behavior of rockfill dams is concerned.

The degradation of particles influences the strength and deformation behavior of coarse granular media [6-16]. Marsal [6] performed triaxial compression tests on coarse granular materials and found out that the most important factor affecting the shear strength and compressibility of the materials is the fragmentation of the granular body during compression and deviatoric loading. All granular aggregates subjected to stresses above normal geotechnical ranges exhibit considerable particle breakage [17-19]; however, particle breakage of rockfills may even occur at low confining pressures [10,20]. Particle crushing causes volumetric

1. *Iran University of Science and Technology, Tehran, P.O. Box 16765-163, Iran.*
2. *Department of Civil and Environmental Engineering, Amirkabir University of Technology, Tehran, P.O. Box 01232747, Iran.*
3. *Department of Civil and Environmental Engineering, Carleton University, Ottawa, Ontario, K1S 5B6, Canada.*
*. *Corresponding author. E-mail: soroush@aut.ac.ir*

Received 27 June 2009; received in revised form 17 October 2009; accepted 20 February 2010

contraction in drained loading and pore pressure build up in undrained loading [21].

Varadarajan et al. [11] investigated the behavior of two dam site rockfill materials in triaxial compression testing; the first material consisted of rounded particles, and the second of angular particles. They observed that the volume change behavior of the two rockfills is significantly different. The rounded material exhibited continuous volume contraction, while the angular materials dilated after initial compression in volume. Also, they observed that a greater degree of particle breakage occurs with angular and larger particles because of the greater force per contact.

The two major factors governing the shear resistance of rockfill materials are interlocking between particles and particle breakage. The effect of increase in interlocking is to increase the shearing resistance, while the effect of breakage of particles is vice versa. Obviously, angular particles are more susceptible to breakage than rounded particles. Alluvial materials at high confining pressures show an increase in the angle of shearing resistance as the size of the particles increases [11,22,23], whereas materials produced from rock blasting show a decrease in the angle of shearing resistance as the size of the particles increases [11,24].

This paper studies the behavior of a number of angular and rounded rockfill materials by conducting large-scale triaxial testing, as well as numerical modeling, using the elasto-plastic Hardening Soil Model [25]. The numerical modeling enables one to predict the stress-strain-volumetric behavior of the materials during shearing.

MATERIALS PROPERTIES

The materials under study are from the shell of eleven rockfill dams constructed or under construction in Iran. These materials lie essentially in two distinct categories: river alluvium, which are mainly rounded or subrounded, and particles produced from the blasting of rock quarries, which are mainly angular or subangular. The above two types of material will be referred, hereafter, in the paper, respectively, as "alluvium" and "blasting" materials. Table 1 summarizes the materials characteristics including rockfill type, mineralogy, size distribution, Loss Angeles abrasion (ASTM C 535), Point Load Strength index (ASTM D 5731), dry density and optimum water content. The maximum dry densities are estimated according to ASTM D1557. For the purpose of brevity, the names of the materials are introduced with their abbreviations.

EXPERIMENTAL PROGRAM

The gradations of the materials for triaxial testing are derived using the parallel gradation modeling technique with a maximum particle size of 50 mm, which is 1/6 of the diameter of the triaxial cell, as shown in Figure 1. The ranges of confining pressure are chosen according to the stress levels in the dams (50 kPa to 1500 kPa). Consolidated Drained (CD) triaxial testing is conducted on the modeled rockfill specimens with dimensions of 300 mm in diameter and 600 mm in height, using the large-scale triaxial equipment at the Geotechnical Department of Build-

Table 1. Characteristics of rockfill materials used in large-scale triaxial testing.

	Material	**Dam**	**Symbol**	**Passing 39.2 mm (%)**	**Passing 25.4 mm (%)**	**Passing 4.75 mm (%)**	**Passing 0.2 mm (%)**	**Los Angeles Abrasion (LA) (%)**	**Point Load Index (I_s)**	**γ_d (95%) (kN/m^3)**	**W_{opt} (%)**
Blasting	Lime stone	Roodbar	BLR[a]	96	84	38	8	30	2.11	21	7.9
	Sand stone	Vanyar	BSV	96	84	38	8	32	2.75	20.8	9.7
	Andesibasalt	Sabalan	BABS	95	72	37	4	28	5.45	21.1	4.5
	Dasite	Zonoz	BDZ	80	72	37	10	20	5.42	21	7.1
	Andesite	Aydoghmosh-G1	BAA1	96	84	37	8	19	3.95	21.8	6.5
		Aydoghmosh-P	BAA2		91	63	0			21.8	
	Lime stone	Siah Bisheh	BLS1	95	85	43	5.5	40	2.75	$21^{b,c}$	5.33
			BLS2							21.5^{b}	
Alluvium	Andesi-Dasite	Yamchi-G1	AADY1	97.5	91	62	10	32	NIA[d]	20.5	9
		Yamchi-G2	AADY2		70	35	7				
	Andesi-Basalt	Ghale-Chai	AABG	92	78	43	10	26	NIA	21.4	9.9
	Deurite-Basit	Sahand-G1	ADBS1	97	91	62	10	46	NIA	20.5	9
		Sahand-G2	ADBS2	96	84	37	8				
	Andesite	Aydoghmosh-G2	AAA	82	73	25	1	19	NIA	22.3	7.4

a: BLR: Stands for Blasting Limestone Roodbar; b: Rate of loading: 1 mm/min; c: γ_d (92%); d: NIA: No Information Available.

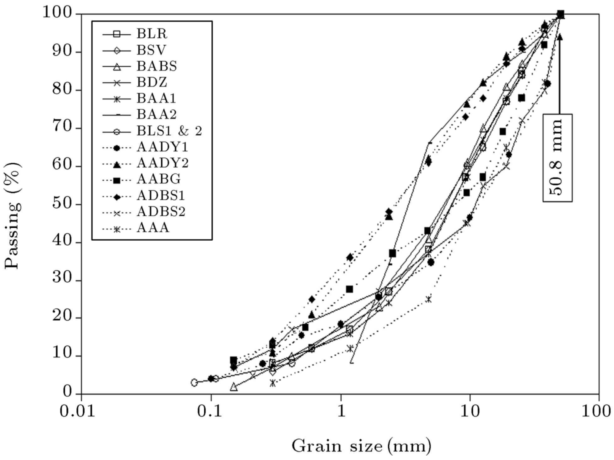

Figure 1. Gradations of the modeled rockfill materials.

ing and Housing Research Center (BHRC), Tehran, Iran.

TESTING PROCEDURE

For each of the specimens, the quantity of various sizes of gain required to achieve the gradation of the modeled rockfill materials for having the specimen at more than 95% maximum dry density is determined by weight. The individual fractions are mixed with distilled water to the optimum moisture content. The specimen materials are divided into six equal parts and prepared in six layers inside a split mold. Each of the layers is compacted using a vibrator with a frequency of 60 cycles/s. After passing CO_2 and applying vacuum, the specimen is saturated to more than 95% (Skempton B-value more than 95%) by allowing water to enter through the base of the triaxial cell and remove the air bubbles. The specimen is subjected first to the required consolidation pressure and then is sheared to failure by applying axial loading at a rate of 0.5 mm/min. A few tests are repeated to verify the reproducibility of the results. Axial loading, vertical displacements and volume changes are monitored and recorded at periodic intervals during the tests.

TESTS RESULTS

Immediate Results

Stress-strain-volume change behaviors of eight modeled blasting rockfill materials subjected to triaxial testing are shown in Figures 2 to 9. It is observed that, in general, axial strain at failure increases with an increase in confining stress. All the blasting materials showed mixed trends (dilation and compression) in their volume change behavior, depending on their confining pressures.

The stress-strain-volume change behaviors of five alluvium rockfill materials are shown in Figures 10

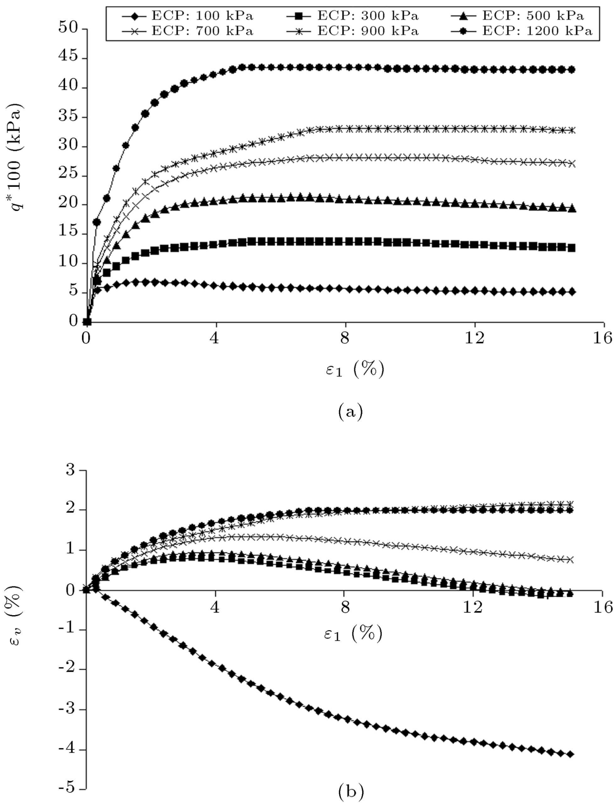

Figure 2. Stress-strain-volume change relationships of BLR.

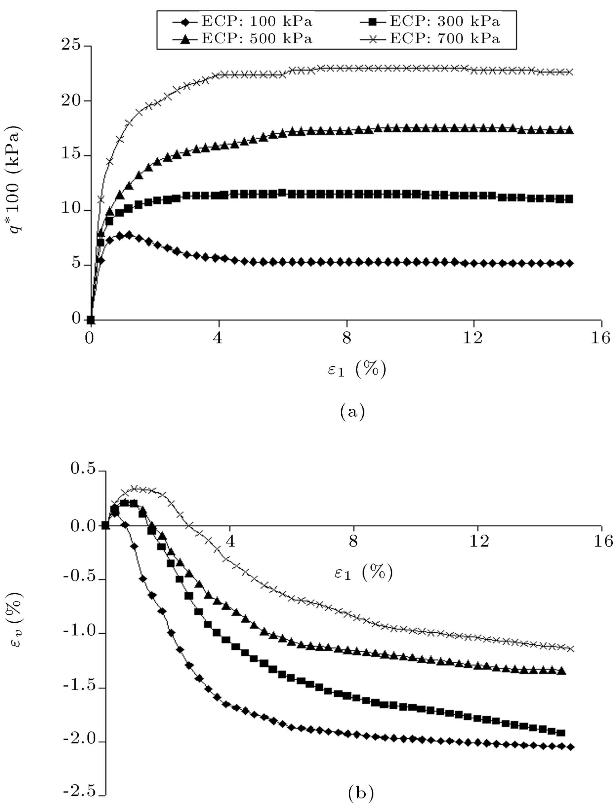

Figure 3. Stress-strain-volume change relationships of BSV.

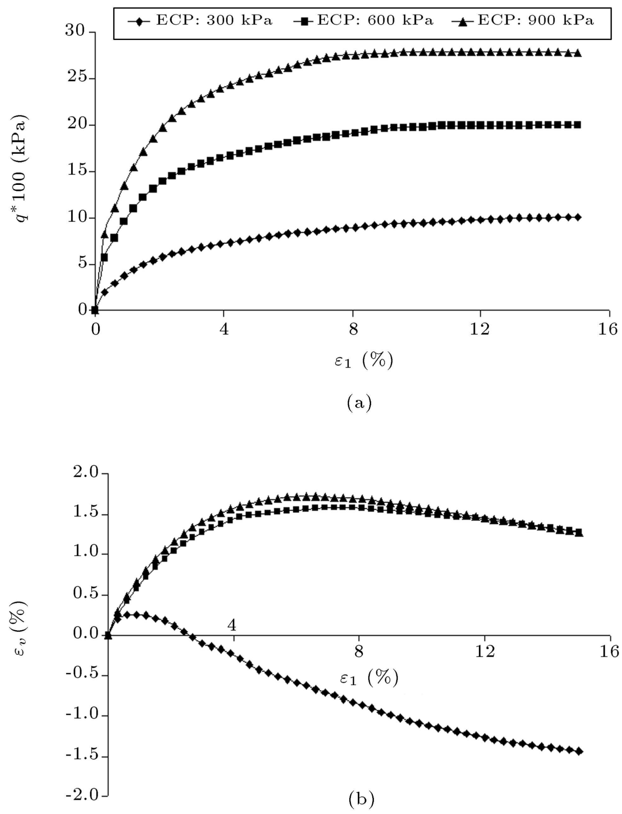

Figure 4. Stress-strain-volume change relationships of BABS.

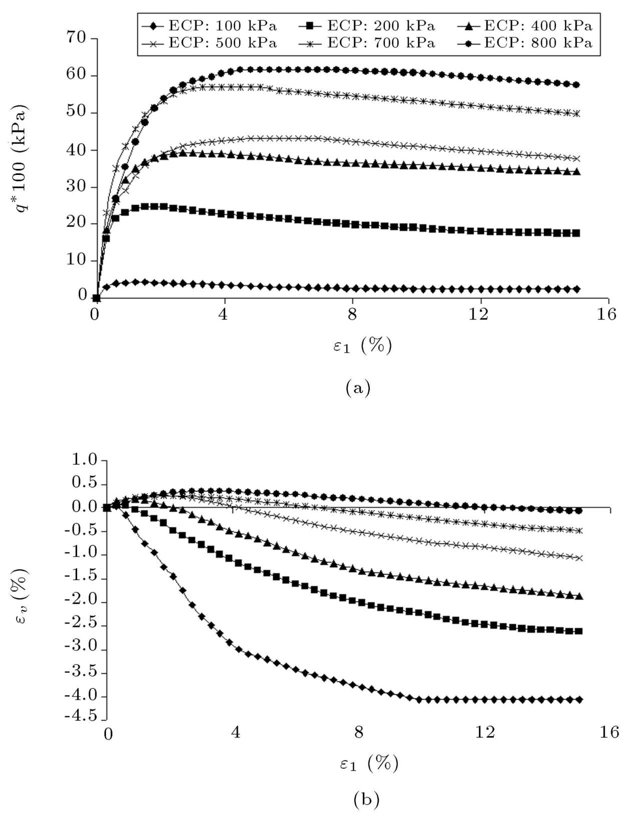

Figure 5. Stress-strain-volume change relationships of BDZ.

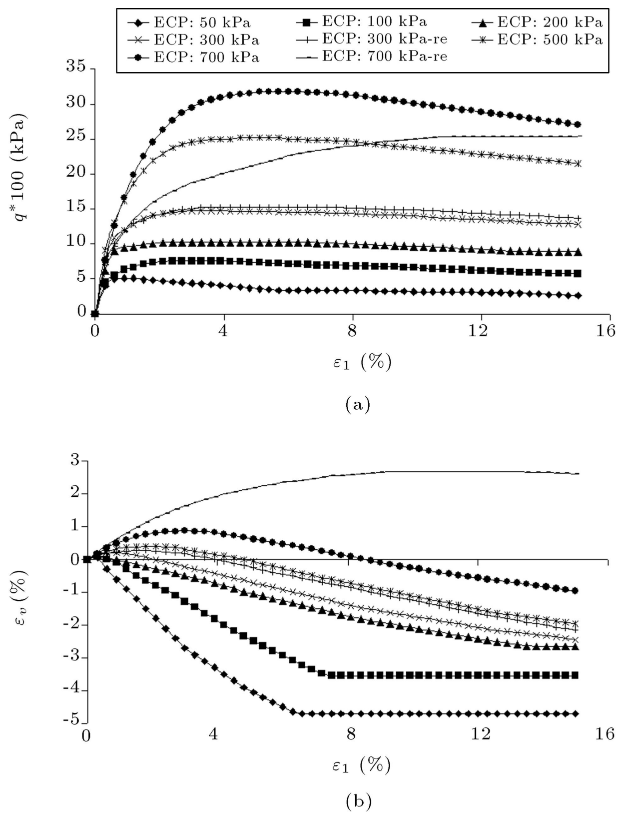

Figure 6. Stress-strain-volume change relationships of BAA1.

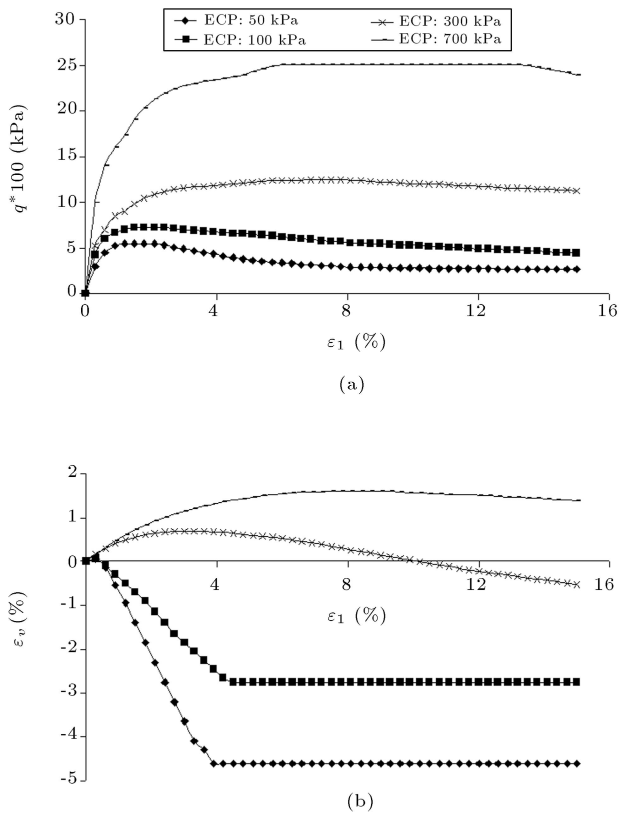

Figure 7. Stress-strain-volume change relationships of BAA2.

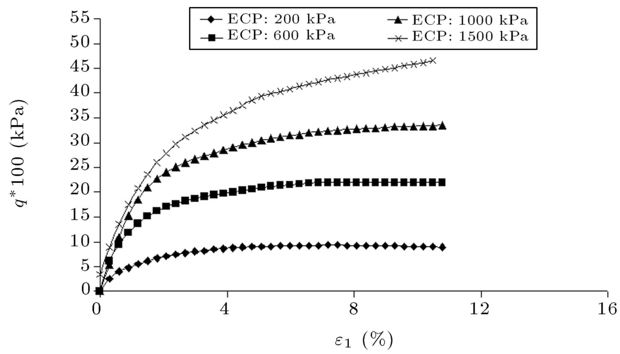

(a)

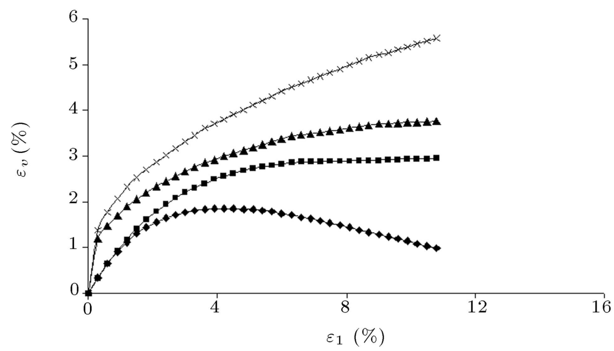

(b)

Figure 8. Stress-strain-volume change relationships of BLS1.

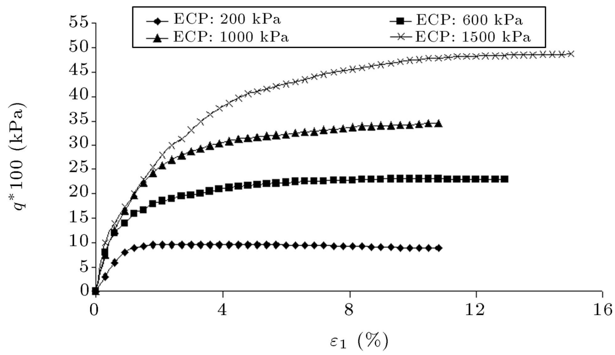

(a)

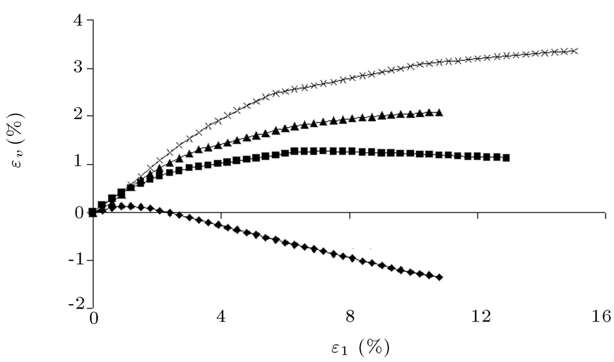

(b)

Figure 9. Stress-strain-volume change relationships of BLS2.

to 15. In these materials, axial strain at failure also increases with confining pressure. The dilation in volumetric strain decreases considerably with an increase in confining pressure.

In these high compacted specimens, a leveling out of the $\varepsilon_v : \varepsilon_1$ behavior occurs in some of the specimens at low confining pressures due to strain localization. At high confining pressures, the highly compacted specimens bulge uniformly in the vicinity of peak stress and develop complex multiple symmetrical radial shear bands at higher axial strain levels [26].

Compiled Results

The compiled tests results of the tests, such as volumetric strain at maximum shear stress $(\varepsilon_v)q_{\max}$, effective internal friction angle at maximum shear stress (ϕ'), ratio of maximum deviator stress to confining pressure ($\frac{q_{\max}}{\sigma_3'}$) and Marsal's breakage index (B_g) [6] are presented in Table 2. This table contains also a number of other parameters, which will be referred to in the coming sections.

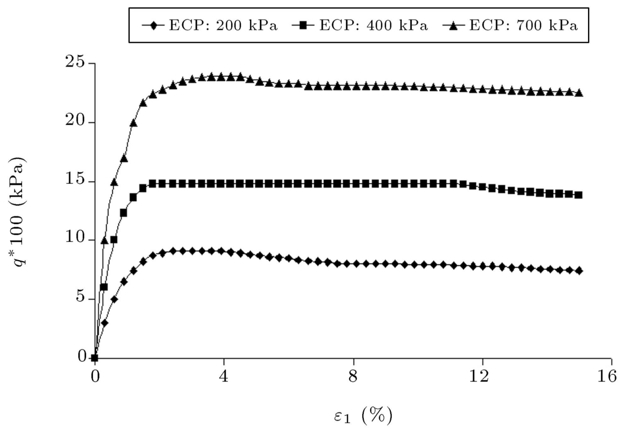

(a)

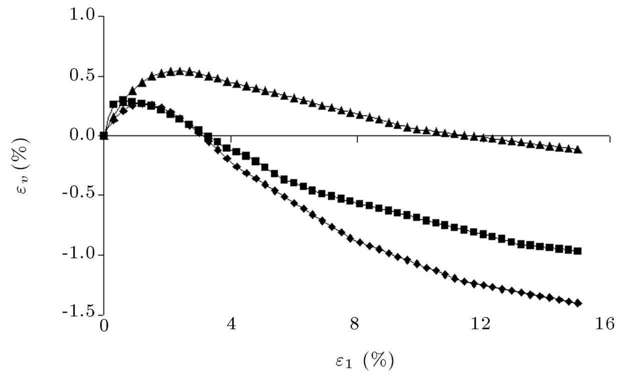

(b)

Figure 10. Stress-strain-volume change relationships of AAY1.

Table 2. Results of triaxial tests and numerical modeling on rockfill materials (continued).

Rockfill	σ'_3 (kPa)	$(\varepsilon_v)q_{\max}$ (%)	ϕ'° (Peak)	$q_{\max}/\sigma'_3$	B_g (%) (at Failure) Test	ϕ'° (Modeling)	ψ° (Modeling)	E_{50}^{ref} *1000 (kPa)	E_{oed}^{ref} *1000 (kPa)	E_{ur}^{ref} *1000 (kPa)
BLR	100	-1	50.4	6.7	NIA[a]	48.5	16	400	390	1200
	300	0.9	45.6	5	NIA	42	2	200	110	600
	500	1	42.6	4.2	11	42	2	200	110	450
	700	1.3	42.4	4.14	12	40	2	150	80	450
	900	2	41.3	3.88	13.5	40	0	150	80	450
	1200	2	39.9	3.58	NIA	38	0	150	70	450
BSV	100	-0.05	53.1	8	NIA	51	19	390	300	1170
	300	-1.2	41.8	4	NIA	40	15	260	200	780
	500	-1.2	40.0	3.6	11	38	12	200	200	600
	700	-1	39.2	3.43	12	38	8	200	247	600
BABS	300	-1.5	38.7	3.33	5.5	38	11	55	116	165
	600	1.4	38.2	3.25	10	38	0	100	60	300
	900	1.5	37.5	3.11	14	38	1	100	6	300
BDZ	100	-0.5	43.0	4.3	NIA	42	19	250	202	750
	200	-0.5	59.5	12.5	NIA	57	13	800	774	1610
	400	-0.2	56.1	9.75	NIA	54.5	6	800	786	2400
	500	-0.1	54.2	8.6	NIA	52.5	4	600	512	1800
	700	0.2	53.4	8.14	NIA	52.5	3	600	588	1800
	800	0.3	52.6	7.75	NIA	51	2	450	434	1350
BAA1	50	-0.08	56.7	10.2	NIA	54.5	22	750	497	2250
	100	-1.4	52.1	7.5	NIA	51	16	400	393	1200
	200	-0.75	46.1	5.15	NIA	45	9	370	362	1110
	300	-0.5	45.3	4.93	4	44.5	7	330	300	1110
	500	0	45.9	5.1	5	44	5	300	200	900
	700	0.48	44.1	4.57	5	43	3	200	120	600
BAA1-repeated	300	0	45.3	4.93	NIA	44.5	5	330	300	990
	700	2.7	39.9	3.57	NIA	39	-3.5	100	65	250
BAA2	50	-2	57.8	11	NIA	55	23	450	319	2250
	100	-1.3	51.1	7	NIA	51	17	400	393	1200
	300	0.5	42.5	4.17	NIA	41	4	150	100	400
	700	1.6	39.9	3.57	2	39	0	150	85	400
BLS1	200	1.5	44.4	4.65	4.8	42.5	1.5	75	47	200
	600	2.7	40.4	3.69	6.91	40	0	80	40	160
	1000	3.3	38.1	3.23	7.55	38	-2	80	41	160
	1500	5	36.9	3	10.07	36	-8	70	35	160
BLS2	200	-0.1	45.0	4.84	5.1	43.5	5	250	244	750
	600	1	41.0	3.82	6.43	41	1	150	85	300
	1000	1.8	39.0	3.4	8.25	39	0	120	70	240
	1500	3	38.0	3.2	12.86	37	-2.5	100	60	200
AADY1	200	0	43.8	4.5	NIA	43	6	250	210	700
	400	0	40.7	3.75	NIA	40.2	5	250	210	700
	700	0.5	39.0	3.4	7.7	38.5	2	250	200	700

a: NIA: No Information Available.

Other parameters of the Hardening Soil model: $v_{ur} = 0.25$, $p^{\text{ref}} = 500$ kPa, $m = 0.35$, $c := 0$, $R_f = 0.9$, $k_0^{nc} = 1 - \sin\phi$.

Table 2. Continued.

Rockfill	σ'_3 (kPa)	$(\varepsilon_v)q_{\max}$ (%)	ϕ'° (Peak)	$q_{\max}/\sigma'_3$	B_g (%) (at Failure) Test	ϕ'° (Modeling)	ψ° (Modeling)	E_{50}^{ref} *1000 (kPa)	E_{oed}^{ref} *1000 (kPa)	E_{ur}^{ref} *1000 (kPa)
ADDY2	200	-0.2	38.2	3.25	5.3	37	2	70	31	300
	400	0.75	40.7	3.75	NIA	40	4	250	106	1000
	700	0.2	39.9	3.57	6.3	39.5	6	150	178	450
ADDY2-Repeated	200	0.2	37.4	3.1	NIA	37	2	70	30	300
	400	0.2	41.3	3.875	NIA	40	9	172	172	700
	700	0.4	40.5	3.71	NIA	39.5	6	300	150	600
AABG	100	-0.2	45.6	5	2.5	44.3	17	750	722	2250
	400	-0.6	38.2	3.25	4	38	9.5	250	250	750
	700	-1	36.9	3	5.9	36	9.5	150	230	450
ADBS1	200	0	44.9	4.8	NIA	45	14.5	370	300	1200
	400	-0.35	45.6	5	NIA	44.5	12	360	270	1020
	700	0	42.4	4.14	NIA	41.7	9	300	250	750
ADBS2	200	-0.5	48.2	5.85	NIA	46.5	20	400	300	1200
	400	0	43.0	4.3	NIA	42	10	400	300	1200
	700	0.85	39.9	3.57	3.1	39	2	200	120	500
AAA	300	0.1	41.5	3.93	NIA	40	5.5	250	160	750
	500	-0.3	47.2	5.5	NIA	45.3	12	500	300	1500
	700	0	43.0	4.28	NIA	42	8	400	300	900

a: NIA: No Information Available.

Other parameters of the Hardening Soil model: $v_{ur} = 0.25$, $p^{\text{ref}} = 500$ kPa, $m = 0.35$, $c := 0$, $R_f = 0.9$, $k_0^{nc} = 1 - \sin\phi$.

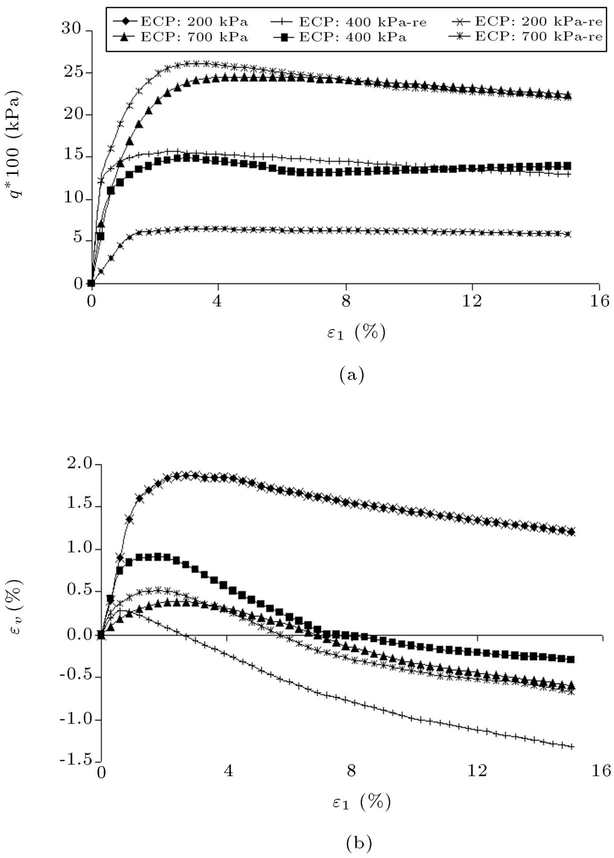

Figure 11. Stress-strain-volume change relationships of AAY2.

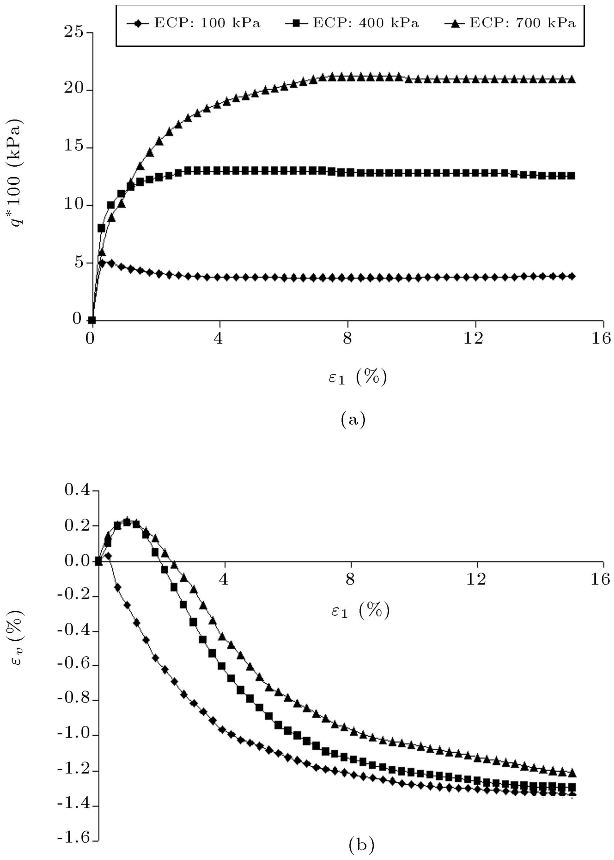

Figure 12. Stress-strain-volume change relationships of AABG.

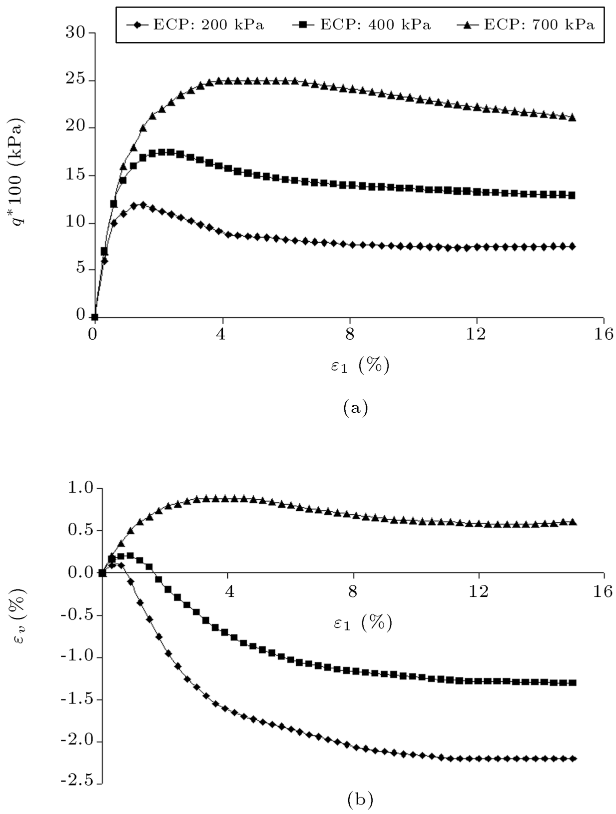

Figure 13. Stress-strain-volume change relationships of ADBS1.

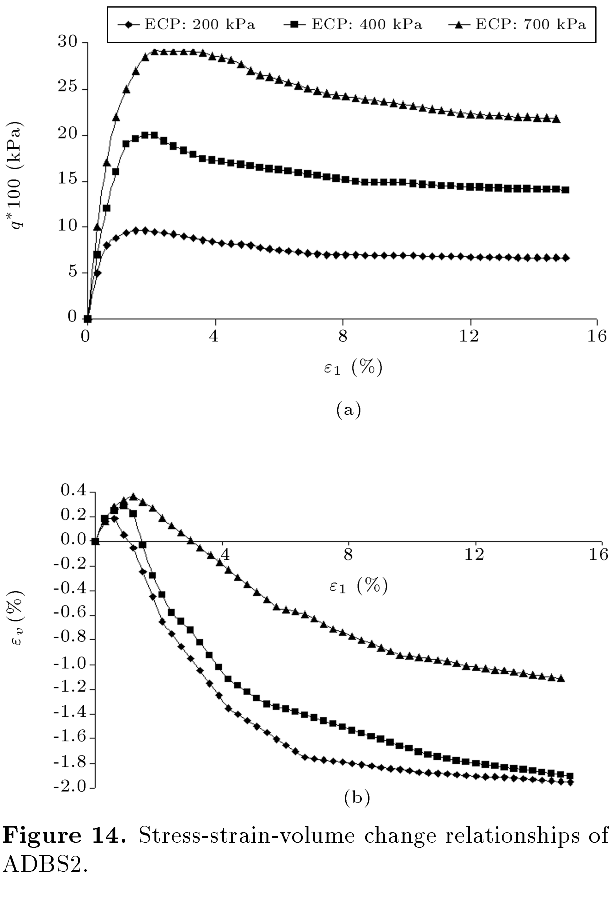

Figure 14. Stress-strain-volume change relationships of ADBS2.

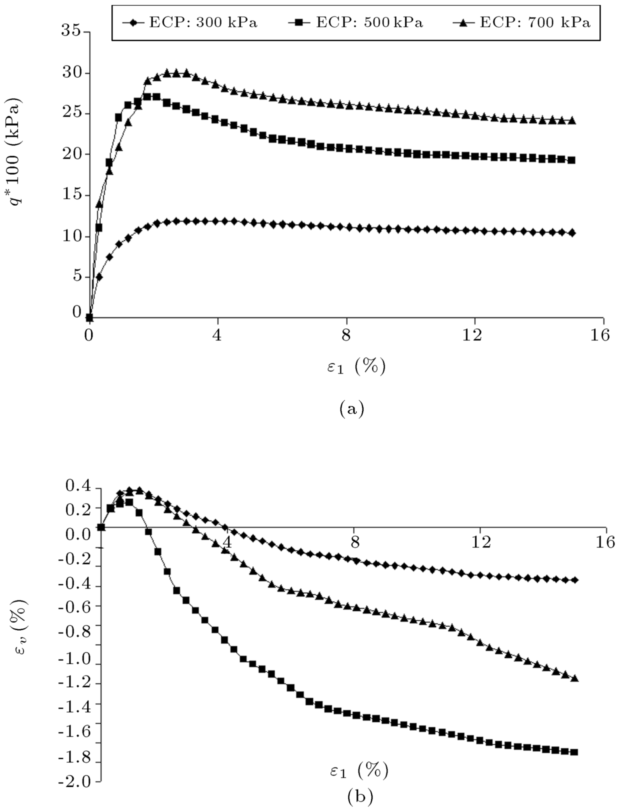

Figure 15. Stress-strain-volume change relationships of AAA.

$(\varepsilon_v)q_{\max} : \sigma_3$

Variations of the volumetric strain at maximum shear stress $(\varepsilon_v)q_{\max}$ versus confining pressure (σ_3') for the blasting and alluvium materials are shown in Figure 16. This figure indicates that for almost all of the blasting materials, $(\varepsilon_v)q_{\max}$ is negative (i.e., dilative behavior) at low confining pressures and positive at high confining pressures (i.e., contractive behavior). The only exception is BSV, in which $(\varepsilon_v)q_{\max}$ remains negative, even for high confining pressures. The variations of $(\varepsilon_v)q_{\max}$ with confining pressures for the alluvium materials are less pronounced, and range from -1% to +1%; whereas the variations for the blasting materials are more, and range from -2% to +5%.

$\phi' : \sigma_3$

The variations of internal friction angle versus confining pressure for the blasting and alluvium materials are presented in Figure 17. Friction angles are calculated for each single confining pressure, assuming $c = 0$ and using the following equation:

$$\sin\phi' = \frac{\sigma_1' - \sigma_3'}{\sigma_1' + \sigma_3'}. \tag{1}$$

Figure 17a indicates that the internal friction angle of the blasting materials decreases with increasing of the

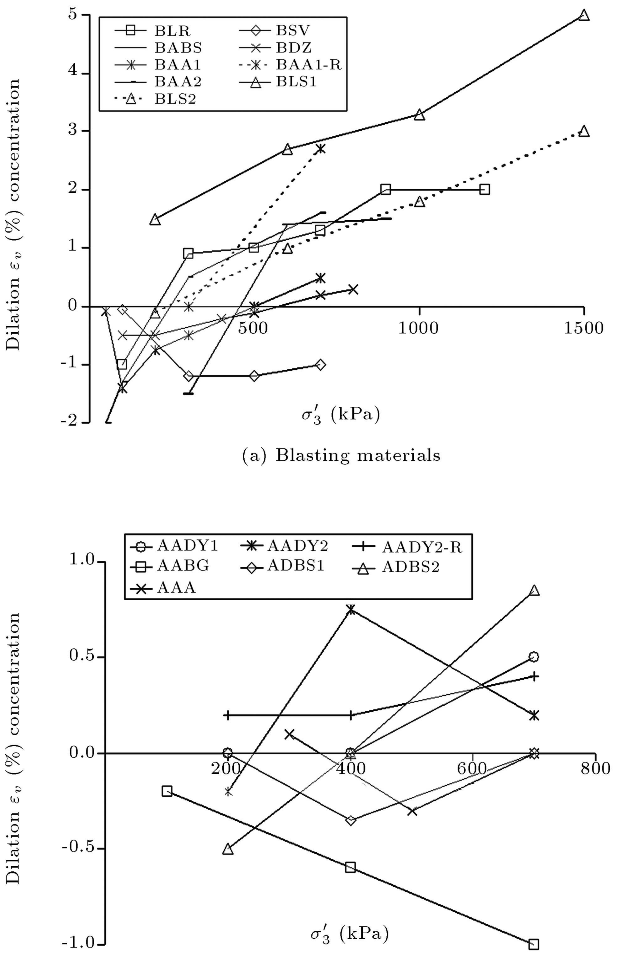

(a) Blasting materials

(b) Alluvium materials

Figure 16. Volumetric strain at maximum shear stress versus confining pressure.

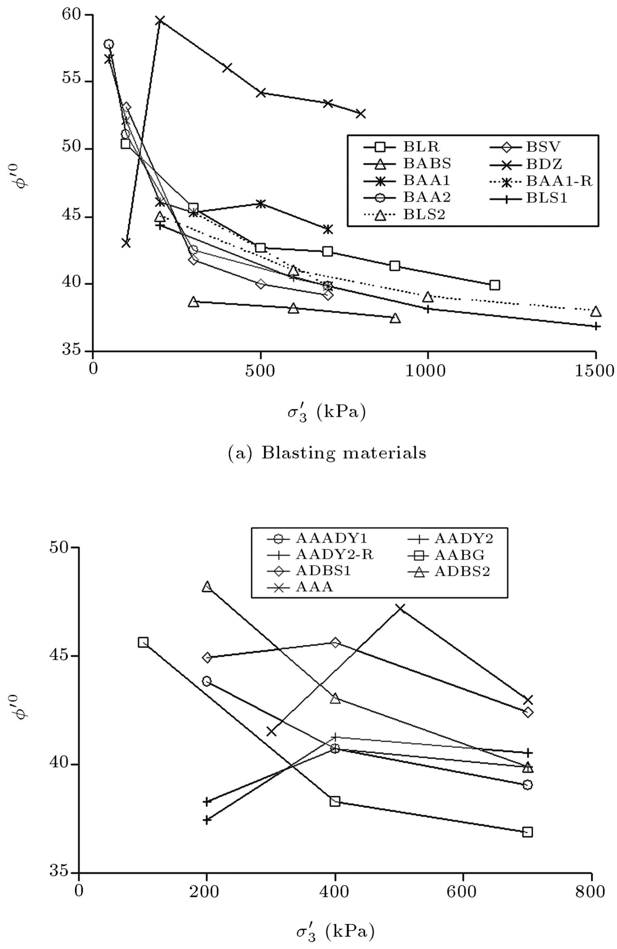

(a) Blasting materials

(b) Alluvium materials

Figure 17. Internal friction angle versus confining pressure.

confining pressure. This is, in fact, due to the effect of particle breakage. The behavior of BDZ materials is an exception in which the internal friction angle first increases sharply from 43° for $\sigma'_3 = 100$ kPa to 59° for $\sigma'_3 = 200$ kPa, then ϕ' decreases moderately to about 53° for $\sigma'_3 = 800$ kPa. For this material, it seems that particle breakage did not happen in the lower stress levels, and that strain localization also occurred very early before the peak, corresponding to a non-homogeneous strain at low confining pressures. At higher stress levels, the amount of softening decreased and some breakage occurred, leading to a decrease in ϕ'; however, it still remains higher than the initial ϕ' at $\sigma'_3 = 100$ kPa. This behavior may be attributed to the fact that this material is relatively hard and stiff, as indicated by its Los Angeles abrasion and point load index, I_s (Table 1). Generally, the internal fiction angle for blasting materials ranges between 59° to 38° for the confining pressures ranging from 50 to 1500 kPa.

Figure 17b shows that the internal friction angle for some of the alluvium materials (e.g. AADY2, ADBS1 and AAA) increases, due to less interlocking, with confining pressures up to 400-500 kPa, and then decreases due to particle breakage, in the higher confining pressure. In these materials, pre-peak strain localization may have occurred, corresponding to a non-homogeneous strain at low confining pressure, which has led to lower values of internal friction angles. In higher stress levels (up to 400-500 kPa), the degree of softening decreases and, at stress levels higher than 500 kPa, some breakage has also occurred, which resulted in decreasing the friction angle. For ADBS2, AADY1, and AABG alluvium materials, continuous decreases in the internal friction angle are observed with an increase in the confining pressures. Generally, the internal friction angle of the alluvium materials for the confining pressures of 100-700 kPa ranges between 49°-37°.

In general, the reduction rate of ϕ' for the blasting materials at low confining pressures is much higher than the same rate for the alluvium materials.

Data presented in Tables 1 and 2 suggests that particle gradation has significant effects on the value of the internal friction angle for both blasting and alluvium materials. Generally, ϕ' for blasting materials subjected to a specific confining pressure decreases with an increase in the size of the particle. For example, the internal friction angle decreases by changing from BAA1 to BAA2 grading (see Figure 1). A similar trend is obvious for the alluvium materials; for example, ϕ' decrease by changing from AADY1 to AADY2 or from ADBS1 to ADBS2 grading. The above behavior may be attributed to the fact that particle breakage potential in materials with relatively larger particles is comparatively higher.

Effect of Point Load Index and Los Angeles Abrasion

Individual particle strength is one of the factors that affects the shear strength of the rockfill materials, in particular, as the particle is subjected to high interparticle stresses during shearing. The strength of rock particles is usually evaluated by the point load test (ASTM D5731).

Figure 18 presents variations of ϕ' versus the ratio of Point Load index to Los Angeles abrasion ($\frac{I_s}{\text{LA}}$) for each of the blasting materials. As expected, stiff materials have higher friction angles.

Particle Breakage

Breakage of the particles was observed during the triaxial tests. The breakage is usually expressed quantitatively by the breakage index, B_g [6]. The value of B_g is calculated by sieving the sample using a set of sieves (50 to 0.075 mm) before and after testing. The percentage of particles retained in each sieve is determined at both stages. Due to breakage of particles, the percentage of the particles retained in large size sieves will decrease and the percentage of particles retained in small size sieves will increase. The sum of the decreases will be equal to the sum of increases in the percentage retained. The decrease (or increase) is the value of the breakage factor, B_g.

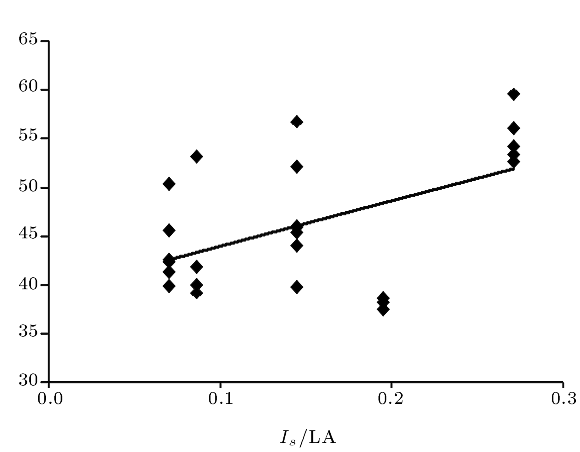

Figure 18. Variation of ϕ' versus I_s/LA for the blasting materials.

Figure 19 shows variations of the maximum principle stress ratio, $(\frac{\sigma'_1}{\sigma'_3})_{\max}$, versus Marsal breakage index (B_g) for the alluvium and blasting materials. As expected, B_g increases as $(\frac{\sigma'_1}{\sigma'_3})_{\max}$ decreases. Consequently, it can be inferred that the friction angle decreases with an increase in B_g (see also Table 2).

Figure 20 presents variations of breakage index versus confining pressure for the two material types. Although the data are scattered, B_g increases generally as σ'_3 increases, with a slightly higher rate of increase for the blasting materials. The effect of particle size and confining pressure on B_g for the blasting material is more significant than for the alluvium materials [11].

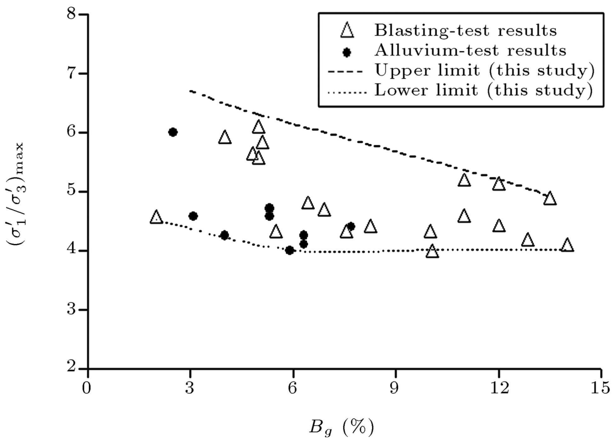

Figure 19. Variations of maximum principle stress ratio $(\frac{\sigma'_1}{\sigma'_3})_{\max}$ versus Marsal breakage index (B_g).

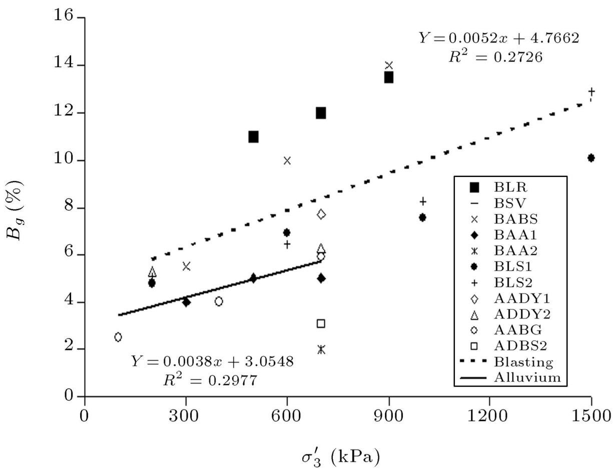

Figure 20. Variations of maximum breakage index (B_g) versus σ'_3.

NUMERICAL MODELING

Constitutive Model

The elasto-plastic Hardening Soil Model [25], adopted in the PLAXIS finite element computer code [27], was employed for numerical analyses. This model uses principles of the hyperbolic model [28] and formulates plastic stresses and strains. The Hardening Soil Model (HSM) supersedes the hyperbolic model by:

(a) Using the theory of plasticity rather than the theory of elasticity;

(b) Including soil dilatancy;

(c) Introducing a yield cap.

The model computes volume changes induced by dilation and employs the yield cap for defining volumetric failures. Some basic characteristics of the model are as follows:

(a) Stress-dependent stiffness according to a power law (input parameter, m);

(b) Plastic straining due to primary deviatoric loading (input parameter, E_{50}^{ref});

(c) Plastic straining due to primary compression (input parameter, E_{oed}^{ref});

(d) Elastic unloading/reloading (input parameters, E_{ur}^{ref}, ν_{ur});

(e) Failure, according to the Mohr-Coulomb model (input parameters, c, ϕ' and ψ). The model relates the dilation angle, ψ, to the volumetric and major principal strains, as follows:

$$\frac{\varepsilon_v}{\varepsilon_1} = \frac{2\sin\psi}{1-\sin\psi}. \tag{2}$$

The verification and modeling of some large-scale triaxial tests and finite element back analyses of the Masjed-E-Soleyman dam showed that the Hardening Soil model is capable of favorably simulating the behavior of rockfill materials [29,30].

Analysis Procedure

In order to substantiate values of the parameters, such as ϕ' and ψ, and to estimate values of the special parameters for the Hardening Soil model (E_{50}^{ref}, E_{oed}^{ref}, E_{ur}^{ref}), we simulated, numerically, the triaxial tests introduced in the foregoing sections. The reference stress for the stiffness in the model was chosen 500 kPa. Based on the simulation results, some empirical correlations are suggested. The HSM is not able to predict the degree of particle breakage at increments of shearing.

Results of Numerical Analyses

Values for the above parameters (ϕ', ψ, E_{50}^{ref}, E_{oed}^{ref} and E_{ur}^{ref}) were selected, so that numerical analyses resulted in the best fits with test results ($q : \varepsilon_1$ and $\varepsilon_v : \varepsilon_1$). The above values are presented in Table 2. Figure 21 compares the stress-strain and volumetric behaviors resulted from analyses for specimen BAA1, which is angular. Figure 22 presents the same comparison for specimen ADBS1, which is rounded. Good agreement between these results and their corresponding test results (Figures 6 and 13, respectively) is evident, indicating that the HSM is capable of capturing the behavior of rockfill materials. These results are typical; favorable results were obtained for the other rockfill type specimens. For each of the materials, a value of ϕ' for the reference stress value of 500 kPa, used for the numerical analyses, is selected two degrees less than the ϕ' value resulted from Equation 1.

Data presented in Table 2 suggests that, generally, the secant stiffness (E_{50}^{ref}), tangent stiffness (E_{oed}^{ref}), and stiffness in unloading and reloading (E_{ur}^{ref}) decrease as σ_3' increases. The behavior of BDZ, AADY2 and AAA

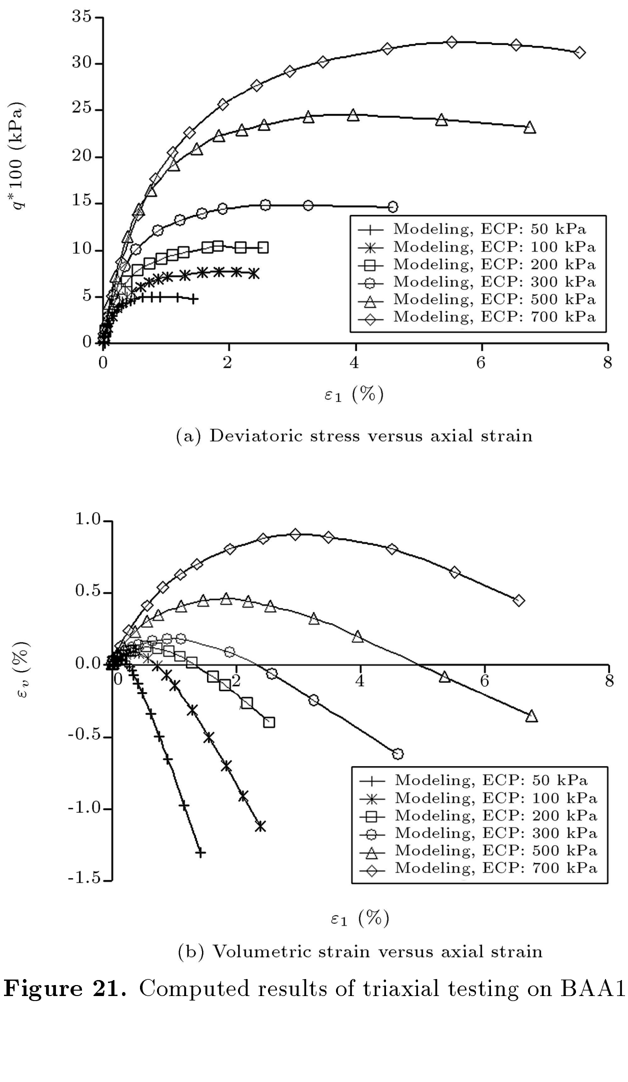

Figure 21. Computed results of triaxial testing on BAA1.

are exceptions, in which the values of the mentioned parameters first increase (probably due to interlocking) with increase of confining pressure, and then decrease (probably due to particle breakage), at higher confining pressure.

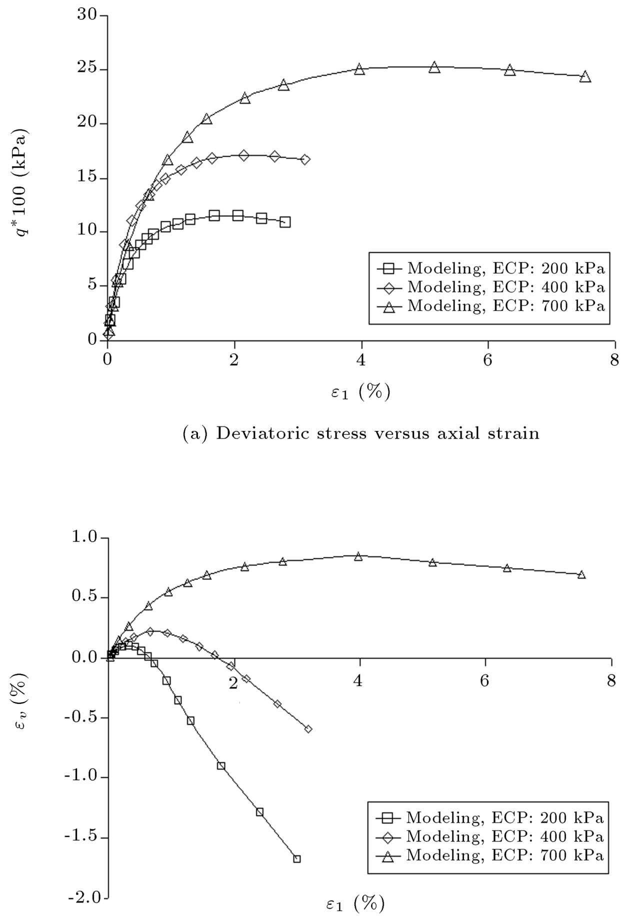

(a) Deviatoric stress versus axial strain

(b) Volumetric strain versus axial strain

Figure 22. Computed results of triaxial testing on ADBS1.

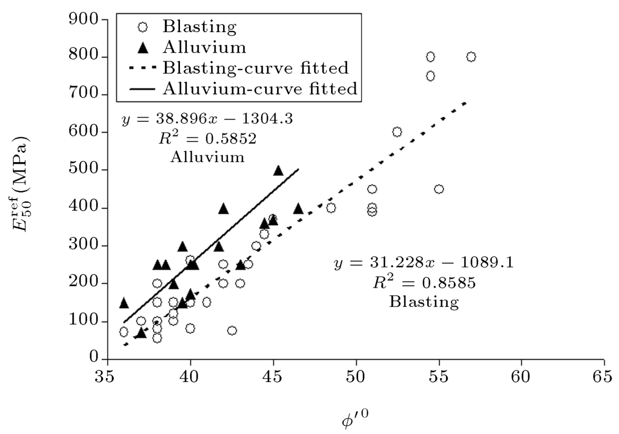

Figure 23. Variation of E_{50}^{ref} versus ϕ' for the blasting and alluvium materials.

Figure 23 shows variations of E_{50}^{ref} versus ϕ' (for reference stress of 500 kPa) for the alluvium and blasting materials separately. Reasonable linear relationships exist for the data. As expected, E_{50}^{ref} increases as ϕ' increases for both types of rockfill material. It is seen that for a given ϕ', E_{50}^{ref} is comparatively higher for the alluvium materials. The following equations may be used for estimating E_{50}^{ref} as a function of ϕ'.

$$E_{50}^{\mathrm{ref}} = 31228\phi' - 1000000, \quad \text{for blasting materials,} \tag{3}$$

$$E_{50}^{\mathrm{ref}} = 39330\phi' - 10^6, \quad \text{for alluvium materials,} \tag{4}$$

where E_{50}^{ref} is in kPa and ϕ' is in degree. Similar trends are obtained for E_{oed}^{ref} and E_{ur}^{ref}.

Figures 24a and 24b show variations of E_{50}^{ref}, respectively, versus E_{ur}^{ref} and E_{oed}^{ref} for the materials. Obviously, linear and almost identical relationships

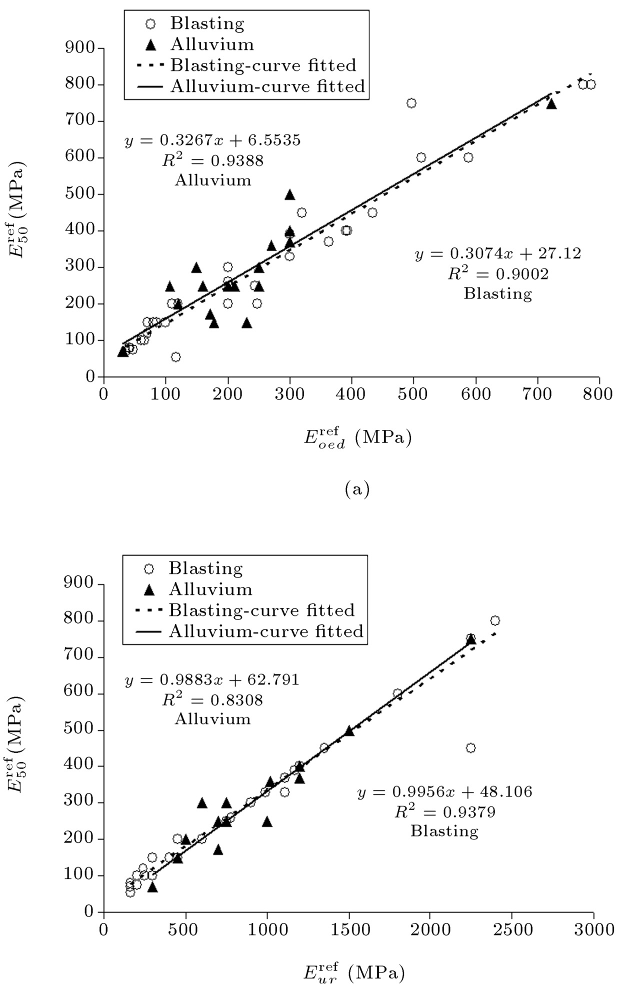

Figure 24. Variation of E_{50}^{ref} versus (a) E_{ur}^{ref} and (b) E_{oed}^{ref} for the blasting and alluvium rockfill materials.

exist between these parameters, as follows:

$$E_{50}^{\text{ref}} = 0.31 E_{ur}^{\text{ref}} + 27000 \text{ (kPa)},$$

for blasting materials, (5)

$$E_{50}^{\text{ref}} = 0.33 E_{ur}^{\text{ref}} + 10000 \text{ (kPa)},$$

for alluvium materials, (6)

$$E_{50}^{\text{ref}} = E_{oed}^{\text{ref}} + 48000 \text{ (kPa)},$$

for blasting materials, (7)

$$E_{50}^{\text{ref}} = E_{oed}^{\text{ref}} + 63000 \text{ (kPa)},$$

for alluvium materials. (8)

SUMMARY AND CONCLUSIONS

This paper presented the results of large scale triaxial testing in drained conditions on a number of rockfill material specimens. Rockfill materials fall basically into two distinct categories:

1. Materials collected from river sediment, which are rounded and/or subrounded (namely alluvium).
2. Materials from rock quarries, which are angular and/or subangular(namely blasting).

The tests results revealed that the strength and deformation parameters of the materials depend on such factors as type and size of particles, confining pressure during tests, Point Load index of the individual particles, and Los Angeles abrasion of the materials. A number of correlations between the above factors and the strength and deformation parameters of the materials are suggested. The main results can be summarized as follows:

- Axial strain at failure of blasting and alluvium rockfills increases with an increase in confining stress.
- The variations of $(\varepsilon_v)q_{\max}$ with confining pressures for the alluvium materials are less pronounced and range from -1% to +1%; whereas the variations for the blasting materials are more, and range from -2% to +5%.
- All the blasting and alluvium materials showed mixed trends (dilation and contraction) in their volume change behavior, depending on their confining pressures. The dilation in volumetric strain decreases considerably with an increase in confining pressure.
- Generally, the internal fiction angle for the blasting materials ranges between 59° to 38° for the confining pressures ranging from 50 to 1500 kPa. The internal friction angle of the alluvium materials for the confining pressures of 100-700 kPa ranges between 49°-37°.
- Generally, ϕ' for the blasting materials subjected to a specific confining pressure, decreases with an increase in the size of the particle.
- As expected, the stiffer materials, as defined by the Point Load Index and Los Angeles Abrasion, have relatively higher friction angles.
- Generally, the internal friction angle of the blasting materials decreases with an increase in confining pressure; whereas the alluvium materials show mixed trends in their friction angle behavior, depending on their confining pressures, stiffness and particle breakage.
- In general, the reduction rate of ϕ' with confining pressure for the blasting materials is much higher at low confining pressures than the same rate for the alluvium materials.
- Generally, B_g increases as σ_3' increases, with slightly higher rate of increase for the blasting materials. The effect of particle size and confining pressure on B_g for the blasting material is more significant than that on the alluvium materials.

The triaxial tests results were also numerically simulated by employing the Hardening Soil Model adopted in the PLAXIS computer code. Reasonable agreements between the simulation results and the tests results were observed, indicating that the Hardening Soil Model is capable of capturing the behavior of rockfill materials. On the basis of the simulation results, the special parameters of the soil model are estimated using a number of correlations.

ACKNOWLEDGMENT

The authors are grateful to the Department of Geotechnical Engineering, BHRC for conducting the tests and for financial support, and to the Ministry of Energy, as the projects' client for providing data for this research. Also, the authors wish to thank the reviewers and referees of this paper for their constructive comments and valuable suggestions.

NOMENCLATURE

B_g	Marsal's breakage index
c	cohesion
CD	Consolidated Drained

E_{50}^{ref}	secant stiffness in standard drained triaxial test
E_{oed}^{ref}	tangent stiffness for primary oedometer loading
E_{ur}^{ref}	stiffness in unloading and reloading
I_s	point load index
m	exponent factor for stress-level dependence of stiffness
P_{ref}	reference stress for stiffness
R_f	failure ratio
W_{opt}	optimum water content
γ_d	dry density
ν_{ur}	Poisson ratio for unloading/reloading
ϕ'	effective friction angle at maximum shear stress
ψ	dilation angle
q	deviatoric stress
σ_3'	effective minor principal stress
LA	Los Angeles abrasion
σ_1'	effective major principal stress
ϕ'_{modeling}	simulated internal friction angle
ε_1	major principal strain
ε_v	volumetric strain

REFERENCES

1. Zeller, J. and Wullimann, R. "The shear strength of the shell materials for the Ge-Schenenalp dam, Switzerland", *Proc., 4th Inst., J. SMFE, London*, **2**, pp. 399-404 (1957).
2. Lowe, J. "Shear strength of coarse embankment dam materials", *Proc., 8th Int. Congress on Large Dams*, **3**, pp. 745-761 (1964).
3. Fumagalli, E. "Tests on cohesionless materials for rockfill dams", *J. SMFE, ASCE*, **95**(1), pp. 313-332 (1969).
4. Frost, R.J. "Some testing experiences and characteristics of boulder-gravel fills in earth dam", *ASTM, STP 523*, pp. 207-233 (1973).
5. Ramamurthy, T. and Gupta, K.K. "Response paper on how one ought to determine soil parameters to be used in design of earth and rockfill dams", *Proc., Indian Geotechnical Conf.*, New Delhi, India, **2**, pp. 15-19 (1986).
6. Marsal, R.J. "Large scale testing of rockfill materials", *J. SMFE, ASCE*, **93**(2), pp. 27-43 (1967).
7. Vesic, A.S. and Clough, G.W. "Behavior of granular materials under high stresses", *J. SMFE, ASCE*, **94**(3), pp. 661-688 (1968).
8. Hardin, B.O. "Crushing of soil particles", *J. SMFE, ASCE*, **111**(10), pp. 1177-1192 (1985).
9. Indraratna, B., Ionescu, D. and Christie, H.D. "Shear behavior of railway ballast based on large-scale triaxial tests", *J. SMFE, ASCE*, **124**(5), pp. 439-449 (1998).
10. Indraratna, B. and Salim, W. "Modeling of particle breakage of coarse aggregates incorporating strength and dilatancy", *Proceedings of the Institution of Civil Engineers*, London, **155**(4), pp. 243-252 (2002).
11. Varadarajan, A., Sharma, K.G., Venkatachalam, K. and Gupta, A.K. "Testing and modeling two rockfill materials", *J. SMFE, ASCE*, **129**(3), pp. 206-218 (2003).
12. Salim, W. and Indraratna, B. "A new elastoplastic constitutive model for coarse granular aggregates incorporating particle breakage" *Can. Geotech. J.*, **41**, pp. 657-671 (2004).
13. Gupta, A.K. "Effect of particle size and confining pressure on breakage and strength parameters of rockfill materials", *Electronic Journal of Geotechnical Engineering*, **14**, Bundle H, pp. 1-12 (2009).
14. Ghanbari, A., Sadeghpour, A.H., Mohamadzadeh, H. and Mohamadzadeh, M. "An experimental study on the behavior of rockfill materials using large scale tests", Bundle G, *Electronic Journal of Geotechnical Engineering*, **13** (2008).
15. Habibagahi, G. and Taherian, M. "Prediction of collapse potential for compacted soils using artificial neural networks", *Scientia Iranica*, **11**(1&2), pp. 1-20 (2004).
16. Hosseini, S.M., Haeri, S.M. and Toll, D.G. "Behavior of gravely sand using critical state concepts", *Scientia Iranica*, **12**(2), pp. 167-177 (2005).
17. Hirschfield, R.C. and Poulos, S.J. "High pressure triaxial tests on compacted sand and undisturbed silt", in *Laboratory Shear Testing of Soils, ASTM, STP*, **361**, pp. 329-339 (1963).
18. Bilam, J. "Some aspects of the behavior of granular materials at high pressures", in *Stress-Strain Behavior of Soils: Proceedings of the Roscoe Memorial Symposium*, Cambridge, R.H.G. Parry and G.T. Foulis, Eds., Co. Ltd., Henley-on-Thames, UK, pp. 69-80 (29-31 March 1971).
19. Lade, P.V., Yamamuro, J.A. and Bopp, P.A. "Significance of particle crushing in granular materials", *J. SMFE, ASCE*, **122**(4), pp. 309-316 (1996).
20. Miura, N. and O-hara, S. "Particle crushing of decomposed granite soil under shear stresses", *Soils and Foundations*, **19**(3), pp. 1-14 (1979).
21. Russell, A.R. and Khalili, N. "A bounding surface plasticity model for sands exhibiting particle crushing", *Can. Geotech. J.*, **41**, pp. 1179-1192 (2004).
22. Sudhindra, C., Venkatachalam, K., Soni, M.L., Sivakumar, N. and Sharma, P. "Large size triaxial shear tests on rockfill materials for design parameters", *Proc. 56th Research and Development Session*, CBIB, Hyderabad, pp. 29-34 (1991).

23. Venkatachalam, K. "Prediction of mechanical behavior of rockfill materials", PhD Thesis, Indian Institute of Technology, Delhi, India (1993).

24. Marachi, N.d., Chan, C.K. and Seed, H.B. "Evaluation of properties of rockfill materials", *J. SMFE*, **98**(1), pp. 95-114 (1972).

25. Schanz, T., Vermeer, P.A. and Bonnier, P.G. "The hardening-soil model-formulation and verification", in *Beyond 2000 in Computational GeotechNICS: Ten Years of Plaxis International*, R.B.J. Brinkgreve, Ed., Balkema, Amsterdam, pp. 281-296 (1999).

26. Alshibli, K.A., Batiste, S.N. and Sture, S. "Strain localization in sand: plane strain versus triaxial compression", *J. Geotech. Geoenviron. Eng.*, **129**(6), pp. 483-494 (2003).

27. Brinkgreve, R.B.J. and Vermeer, P.A. "PLAXIS finite element code for soil and rock analyses", Version 7, Plaxis BV, Delft (1998).

28. Duncan, J.M. and Chang, C.Y. "Nonlinear analysis of stress and strain in soils", *J. SMFE, ASCE*, **96**(5), Proceedings Paper 7513 (1970).

29. Aghaei Araei, A. "Back analysis of deformations induced during first impounding of Masjed-E-Soleyman dam", MS Thesis, Department of Civil and Environmental Engineering, Amirkabir University of Technology, Tehran, Iran (2002).

30. Soroush, A. and Aghaei Araei, A. "Analysis of behavior of a high rockfill dam", *GE Proceedings of the Institution of Civil Engineers (ICE)*, **159**(1), pp. 49-59 (2006).

BIOGRAPHIES

Ata Aghaei Araei is a PhD candidate in the School of Civil Engineering at Iran University of Science and Technology (IUST) and also PhD Researcher at Geotechnical Laboratory of Civil Engineering at The University of Tokyo. He received his MS from the Amirkabir University of Technology (Tehran Polytechnic) in 2002. He is working as a senior geotechnical engineer and head of geotechnical laboratory at Building and Housing Research Center (BHRC) since 2003. Mr. Aghaei-Araei's primary research interests include: (i) Monotonic and dynamic testing on geomaterials, (ii) Microzonation, (iii) Geotechnical equipment construction.

Abbas Soroush is an associate professor in the Department of Civil and Environmental Engineering at the Amirkabir University of Technology (Tehran Polytechnic) since 1997. He received his PhD degree in Geotechnical Engineering under the supervision of Professor N.R. Morgenstern from the Department of Civil and Environmental Engineering, University of Alberta, Canada. His research interests cover a variety of subjects, including numerical modeling of geomaterials and soil structures, especially earth dams. Dr. Soroush is known as an expert in dam engineering and has attended several numbers of international expert panels for reviewing large dams in the country.

Mohammad Rayhani is an Assistant Professor in the Department of Civil and Environmental Engineering at Carleton University. He received his PhD from the University of Western Ontario in 2007. Prior to joining Carleton University in 2009, he worked as a postdoctoral fellow and adjunct professor at Queen's university between 2007 and 2009. He has over 10 years experience in the field of geotechnical engineering and geotechnical engineering research. He has been involved in over 20 engineering projects in Canada and Iran and has experience in foundation investigation and design, landfill barrier design, geotechnical earthquake engineering, embankment dam design and slope stability. Dr. Rayhani's primary research interests include: (i) Landfill barrier systems, (ii) Seismic site response and soil-structure interaction, and (iii) Geotechnical hazards.